

Instanton Theory for Nonadiabatic Tunneling through Near-Barrier Crossings

Ziyan Ye,[†] Eric R. Heller,^{*,‡} Dong H. Zhang,^{¶,§} Jeremy O. Richardson,^{*,||} and Wei Fang^{*,†}

[†]*Department of Chemistry, Shanghai Key Laboratory of Molecular Catalysis and Innovative Materials, State Key Laboratory of Porous Materials for Separation and Conversion, Fudan University, Shanghai 200438, P. R. China*

[‡]*Department of Chemistry, University of California, Berkeley, 94720 Berkeley, USA*

[¶]*State Key Laboratory of Molecular Reaction Dynamics, Dalian Institute of Chemical Physics, Chinese Academy of Sciences, Dalian 116023, P. R. China*

[§]*University of Chinese Academy of Sciences, Beijing 100049, China*

^{||}*Department of Chemistry and Applied Biosciences, ETH Zürich, Zürich 8093, Switzerland*

E-mail: hellere@berkeley.edu; jeremy.richardson@phys.chem.ethz.ch; wei_fang@fudan.edu.cn

Abstract

Many reactions in chemistry and biology involve multiple electronic states, rendering them nonadiabatic in nature. These reactions can be formally described using Fermi’s golden rule (FGR) in the weak-coupling limit. Nonadiabatic instanton theory presents a semiclassical approximation to FGR, which is directly applicable to molecular systems. However, there are cases where the theory has not yet been formulated. For instance, in many real-world reactions including spin-crossover or proton-coupled electron transfer, the crossing occurs near a barrier on a diabatic state. This scenario gives rise to competing nonadiabatic reaction pathways, some of which involve tunneling through a diabatic barrier while simultaneously switching electronic states. To

date, no rate theory is available for describing tunneling via these unconventional pathways. Here we extend instanton theory to model this class of processes, which we term the “non-convex” regime. Benchmark tests on model systems show that the rates predicted by instanton theory are in excellent agreement with quantum-mechanical FGR calculations. Furthermore, the method offers new insights into multi-step tunneling reactions and the competition between sequential and concerted nonadiabatic tunneling pathways.

1 Introduction

Nonadiabatic effects arise when multiple electronic states are involved in chemical reactions or other physical processes, leading to the breakdown of the Born–Oppenheimer approximation.¹ Such effects are widespread in molecular science, with notable examples including spin-crossover reactions in transition-metal chemistry,² charge transfer in biochemistry³ and dynamics through conical intersections in photochemistry.⁴ Simulating nonadiabatic phenomena is critical for understanding important chemical, physical, and biological processes at the molecular level. However, atomistic simulations beyond the Born–Oppenheimer approximation pose significant challenges.⁵

Fermi’s golden rule (FGR)⁶ gives the exact nonadiabatic quantum transition rate in the weak-coupling limit. It has been widely applied to simulate processes like electron transfer⁷ and nonradiative transitions.⁸ However, despite its reliability and broad applicability, FGR suffers from its tremendous computational cost in solving vibrational wave-functions, making its direct application to complex high-dimensional molecular systems unfeasible.

The most widely used rate theory for nonadiabatic processes is the well-known Marcus theory,^{9,10} which can be derived from FGR using classical statistical mechanics for the nuclei and assuming parabolic free-energy surfaces.¹¹ Nonadiabatic transition state theory (NA-TST)^{12–15} goes beyond the assumption of globally parabolic surfaces by identifying the minimum-energy crossing point (MECP) and using the molecular partition functions eval-

uated at the MECP and the reactant minimum. Simple tunneling corrections to NA-TST have been proposed, such as the weak-coupling approximation (WC),^{16,17} which assumes linear diabatic potential-energy surfaces (PESs) along the tunneling coordinate.¹⁷ While this approach is appropriate for the shallow-tunneling regime, it yields qualitatively wrong results in the low-temperature, deep-tunneling regime.^{18,19}

Although semiclassical instanton theory (SCI) was originally formulated within the Born–Oppenheimer approximation,²⁰ it has been generalized to the nonadiabatic case,^{21–24} where it provides a semiclassical approximation to FGR that can be directly applied to multidimensional molecular reactions. The approach is based on Feynman’s path-integral formulation of quantum mechanics²⁵ and estimates the transition rate based on a single optimal tunneling pathway, called an instanton, rather than requiring the evaluation of numerous overlaps between vibrational wavefunctions as in the original FGR. This makes instanton calculations far more computationally efficient than their quantum-mechanical counterparts. SCI predicts rates nearly identical to those from FGR for various model systems,^{21,26} and has been successfully applied to several molecular systems using on-the-fly electronic-structure theory, demonstrating excellent agreement with experimental results and providing evidence that nuclear tunneling may occur even for heavy atoms at room temperature.^{18,19,27–29}

However, the complexity of real-world reactions often challenges the validity of existing nonadiabatic rate theories. Reaction profiles involving the intersection of two double-well potentials, as illustrated in Fig. 1b, are commonly observed in proton-coupled electron transfer (PCET)^{30–32} and spin-crossover systems such as carbenes,³³ nitrenes,^{34–36} diradicals³⁷ and transition-metal complexes.^{15,38–42} Despite the rich literature on nonadiabatic processes, to the best of our knowledge, reaction mechanisms (especially those that involve tunneling) with a near-barrier crossing remain largely unexplored. A major reason is that these systems are challenging for existing nonadiabatic rate theories. For example, NA-TST and WC only utilize local information in the neighborhood of the minimum energy crossing point (MECP), without recognizing the complex shape of the reaction profile. Although these

theories generally suffice at high temperatures for simpler nonadiabatic reactions (as illustrated in Figure 1a), for the intersecting double-well system (Figure 1b), they can only describe the process from R_0 to R_1 (or conversely). Therefore, it has long been believed that reactions occur via a sequential mechanism: first a nonadiabatic process from R_0 to R_1 followed by an adiabatic process to P_1 . However, a concerted deep tunneling path may exist, directly linking R_0 and P_1 , rivaling the conventional sequential picture.

In this work, we apply instanton theory to systematically investigate tunneling mechanisms in nonadiabatic reactions in cases where the crossing occurs close to a barrier top. Surprisingly, the standard nonadiabatic instanton rate expression is found to be not directly applicable to these systems due to an unexpected sign error in the prefactor, which describes fluctuations around the instanton path. In the following, we extend SCI to this “non-convex” regime by analytic continuation. In fact, part of the theory we derive in this work was recently applied to explain the tunneling mechanisms of triplet carbenes.²⁹ Here, we present

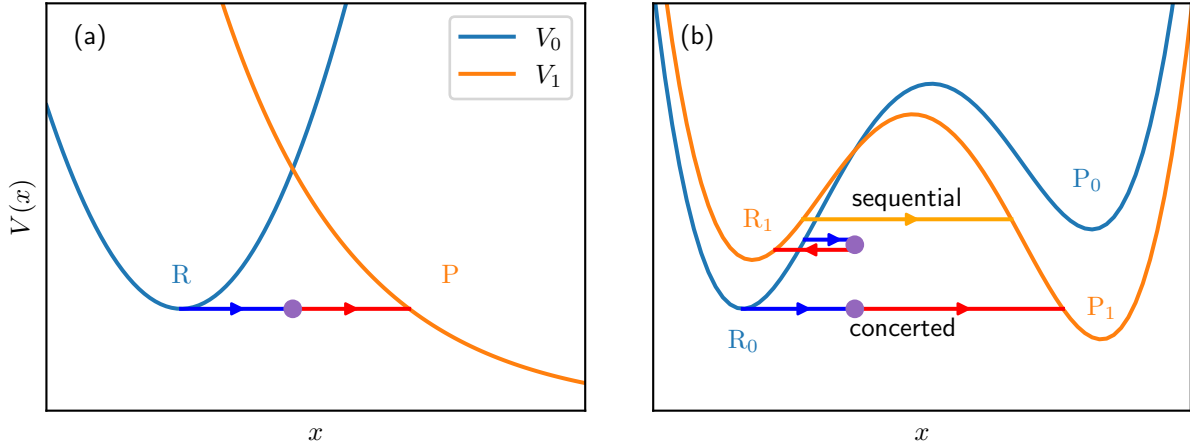


Figure 1: Schematic diagrams of crossing diabatic states (0 and 1) in the convex (a) and non-convex (b) regimes along with the instantons involved. (a) A system without any diabatic barrier. The only possible reaction is the transition from reactants (R) to products (P). The instanton consists of tunneling paths on either state (in blue and red) and changes electronic state at the hopping point (purple dot). (b) A system with a near-barrier crossing. Both potentials exhibit diabatic barriers, which lie in the vicinity of the crossing point. Hence, there exist multiple competing instanton pathways.

a rigorous justification of the approach, provide additional methodological details and introduce extensions to the inverted regime, along with a broader discussion of the scope of the non-convex case.

2 Semiclassical instanton theory

In this section, we briefly summarize the previous derivation of SCI presented in Ref. 23, which is valid in both the normal and inverted regimes. We consider a molecular system with reactant and product diabatic electronic states $|0\rangle$ and $|1\rangle$, whose Hamiltonian is given by

$$\hat{H} = \hat{H}_0 |0\rangle \langle 0| + \hat{H}_1 |1\rangle \langle 1| + \hat{\Delta} (|0\rangle \langle 1| + |1\rangle \langle 0|), \quad (1)$$

where $\hat{\Delta} = \Delta(\hat{x})$ denotes the nonadiabatic coupling between the two states. The nuclear Hamiltonians are given by

$$\hat{H}_n = \frac{\hat{p}^2}{2m} + V_n(\hat{x}), \quad (2)$$

where $n \in \{0, 1\}$, \hat{x} comprises the f nuclear degrees of freedom moving on PES V_n according to their conjugate momenta \hat{p} . The variables are assumed to be mass-weighted such that all degrees of freedom have the same mass, m . In the golden-rule regime, where the coupling $\hat{\Delta}$ is weak, the interaction can be treated perturbatively, leading to the well-known FGR

$$kZ_0 = \frac{2\pi}{\hbar} \sum_{\mu} e^{-\beta E_0^{\mu}} \sum_{\nu} \left| \langle \mu | \hat{\Delta} | \nu \rangle \right|^2 \delta(E_1^{\nu} - E_0^{\mu}), \quad (3)$$

where k is the reaction rate constant, Z_0 is the reactant partition function, $\beta = 1/k_{\text{B}}T$ is the inverse temperature, μ and ν denote vibrational eigenstates on electronic states 0 and 1, and energy conservation is enforced by the δ -function. Equation (3) can be equivalently expressed as an integral of the flux correlation function c_{ff} over time t ,^{43–45}

$$kZ_0 = \int_{-\infty}^{+\infty} c_{\text{ff}}(\tau + it) dt, \quad (4)$$

$$c_{\text{ff}}(\tau + it) = \frac{1}{\hbar^2} \text{Tr} \left[\hat{\Delta} e^{-(\beta\hbar - \tau - it)\hat{H}_0/\hbar} \hat{\Delta}^\dagger e^{-(\tau + it)\hat{H}_1/\hbar} \right], \quad (5)$$

where the integral in Eq. (4) is independent of the imaginary time τ by virtue of Cauchy's integral theorem, provided that the integration contour in the complex-time plane does not enclose any singularities.²⁸

SCI can now be derived as a semiclassical approximation to FGR.^{21,23,26} We expand the trace in Eq. (5) in a basis of position eigenstates and approximate the quantum propagators by the corresponding semiclassical van Vleck propagators^{46,47} to give

$$kZ_0 \sim \frac{1}{\hbar^2} \iiint \Delta(x') \Delta^*(x'') \frac{\sqrt{C_0} \sqrt{C_1}}{(2\pi\hbar)^f} e^{-S/\hbar} dx' dx'' dt, \quad (6)$$

where the total path action $S \equiv S_0(x', x'', \beta\hbar - \tau - it) + S_1(x'', x', \tau + it)$ consists of an action integral along a classical trajectory in complex time z_n on each electronic state

$$S_n(x_i, x_f, z_n) = \int_0^{z_n} \left[\frac{1}{2} m |\dot{x}(u)|^2 + V_n(x(u)) \right] du, \quad (7)$$

with x_i and x_f being the starting and ending points ($x_i = x''$, $x_f = x'$ for $n = 0$, and $x_i = x'$, $x_f = x''$ for $n = 1$), and C_n is defined by the $f \times f$ determinant

$$C_n = \left| -\frac{\partial^2 S_n}{\partial x_i \partial x_f} \right|. \quad (8)$$

The semiclassical instanton rate expression is then obtained by evaluating the integrals in Eq. (6) using the steepest-descent approximation around the instanton, a periodic trajectory satisfying the principle of stationary-action. The resulting rate expression is given by

$$k_{\text{SCI}} Z_0 = \sqrt{2\pi\hbar} \frac{\Delta^2}{\hbar^2} \frac{\sqrt{C_0} \sqrt{C_1}}{\sqrt{C}} \left(-\frac{d^2 S}{d\tau^2} \right)^{-\frac{1}{2}} e^{-S/\hbar}, \quad (9)$$

where all quantities are evaluated at the instanton, which is a stationary point of S with respect to x' , x'' and τ . The coupling is defined as $\Delta \equiv |\Delta(x')| = |\Delta(x'')|$ since typically

$x' = x''$, and the prefactor C is defined by

$$C = \begin{vmatrix} \frac{\partial^2 S}{\partial x' \partial x'} & \frac{\partial^2 S}{\partial x' \partial x''} \\ \frac{\partial^2 S}{\partial x'' \partial x'} & \frac{\partial^2 S}{\partial x'' \partial x''} \end{vmatrix}. \quad (10)$$

The minus sign in front of $\frac{d^2 S}{d\tau^2}$ arises from the Cauchy–Riemann equations, which relate the derivatives with respect to real time t to those with respect to imaginary time τ . Note that in Eq. (9), we write the square roots separately to emphasize that, in this derivation, \mathbf{C}_0 , \mathbf{C}_1 and \mathbf{C} (the matrices corresponding to determinants C_0 , C_1 and C) are each required to be positive definite, while $\frac{d^2 S}{d\tau^2}$ must be negative, in accordance with the steepest-descent method. All of these conditions hold for systems in the normal regime without diabatic barriers.^{19,21,23} The energy of an instanton trajectory can be obtained by taking the derivative of the action

$$\frac{\partial S_n(x_i, x_f, \tau_n)}{\partial \tau_n} = E_n, \quad (11)$$

where $\tau_0 = \beta\hbar - \tau$ and $\tau_1 = \tau$. Instanton theory enforces energy conservation at the hopping point, such that $E_0 = E_1 \equiv E$.

The SCI rate in Eq. (9) can equivalently be written as

$$k_{\text{SCI}} Z_0 = \sqrt{2\pi\hbar} \frac{\Delta^2}{\hbar^2} \sqrt{\frac{C_0 C_1}{-\Sigma}} e^{-S/\hbar}, \quad (12)$$

$$\Sigma = \begin{vmatrix} \frac{\partial^2 S}{\partial x' \partial x'} & \frac{\partial^2 S}{\partial x' \partial x''} & \frac{\partial^2 S}{\partial x' \partial \tau} \\ \frac{\partial^2 S}{\partial x'' \partial x'} & \frac{\partial^2 S}{\partial x'' \partial x''} & \frac{\partial^2 S}{\partial x'' \partial \tau} \\ \frac{\partial^2 S}{\partial \tau \partial x'} & \frac{\partial^2 S}{\partial \tau \partial x''} & \frac{\partial^2 S}{\partial \tau^2} \end{vmatrix}, \quad (13)$$

where all square roots are combined into one and Σ has one negative eigenvalue. Equation (12) will prove more useful for the analytic continuation to the non-convex regime, which we perform in the following section. We thereby follow a similar approach to the analytic continuation of instanton theory to the inverted regime,²⁶ where $\tau < 0$. In that case, \mathbf{C}_1

is negative definite, \mathbf{C} has f negative eigenvalues, and $\mathbf{\Sigma}$ has $f + 1$ negative eigenvalues (see the first two rows in Table 1). Despite these qualitative changes in several components of the prefactor, the total SCI rate expression [Eq. (12)] remains valid, which we will demonstrate to hold also in the non-convex regime.

3 Instanton theory in the non-convex regime

3.1 Sign problem in the non-convex regime

Previously, SCI has been applied to nonadiabatic processes where both diabatic PESs are convex near the crossing seam, as illustrated in Figure 1a. As explained in Section 2, for the convex case, C_0 , C_1 , C , and $-\frac{d^2S}{d\tau^2}$ should all be positive in the normal regime, while the signs of C_1 and C should both be $(-1)^f$ in the inverted regime. However, if either of the two diabatic PESs exhibits a barrier near the crossing point, as illustrated in Fig. 1b, the surface becomes non-convex in that region, potentially altering the signs of the terms in the SCI prefactor. In the following, we take V_0 to be non-convex and V_1 to be convex. The argument extends straightforwardly to cases where both surfaces are non-convex. As a consequence, the diabatic Hessians along the instanton path on V_0 are no longer positive definite, in which case the \mathbf{C} or \mathbf{C}_0 matrix gains one extra negative eigenvalue, while $\frac{d^2S}{d\tau^2}$ becomes positive (Table 1). We name this scenario the “non-convex regime”. We prove that a non-convex V_0 is the necessary condition for this regime to appear in one-dimensional systems and separable multidimensional systems (SI Section S1), as well as in the classical limit for general systems (Appendix A).

As shown in Table 1, instantons in the non-convex regime exhibit significant diversity, making it important to establish a clear categorization. As in convex systems, reactions in non-convex systems can also be classified into Marcus normal and inverted regimes, depending on whether the reactant and product lie on opposite sides or the same side of the crossing seam. Similarly, the distinction between normal-regime and inverted-regime instan-

Table 1: Summary of instantons in the convex and non-convex regimes.

Regime		C_0^*	C_1^\dagger	C	$\frac{d^2 S}{d\tau^2}$	Curvature of V_0 along instantons
Convex	Normal	+	+	+	−	Dominantly positive
	Inverted	+	$(-1)^f$	$(-1)^f$	−	
Non-convex	Type I	Normal	+	−	+	Balanced positive/negative
		Inverted	+	$(-1)^f$	$(-1)^{f+1}$	
	Type II	Normal	−	+	+	Dominantly negative
		Inverted [‡]	−	$(-1)^f$	+	

* For the non-convex instantons, we assume V_0 to be the non-convex PES. The extra minus sign on C_0 would appear on C_1 instead in the type-II normal regime for a system where V_0 is convex and V_1 is non-convex.

† Here we consider the inverted regime where $\tau_1 < 0$. If instead $\tau_0 < 0$, then the $(-1)^f$ on C_1 would appear on C_0 .

‡ Not found in this work.

tons based on whether $\tau > 0$ or $\tau < 0$,^{21,26} remains valid regardless of whether the system is in the convex or non-convex regime. Furthermore, non-convex instantons can be categorized into type I and type II, depending on whether the extra minus sign appears in C or C_0 . The extra minus in C_0 is associated with Morse’s theorem,⁴⁷ which implies that C_0 changes its sign every time the trajectory goes through a conjugate point. In classical mechanics, a conjugate point is a point along a trajectory where nearby paths, representing slight variations in motion, meet up again, signaling that the original path might stop being the most stable or unique solution beyond that point. Hamilton’s principle requires that a classical trajectory is a stationary point of the action. For a (finitely) short trajectory, this reduces to the least-action principle.⁴⁸ However, as the trajectory progresses, it will switch from a least action point with $C_0 > 0$ to a first-order saddle point of the action with $C_0 < 0$. *

Although the distinction between type I and II non-convex instantons is theoretically significant, type II instantons exhibit no distinct behaviors compared to type I instantons. Instead, a more straightforward and practical categorization of non-convex instantons is

*If the trajectory terminates at its conjugate point, which marks the boundary between the region where the trajectory is a minimum of the action and the region where it becomes a saddle point, the second variation of the action exhibits a zero eigenvalue and thus $C_0 \rightarrow \infty$.

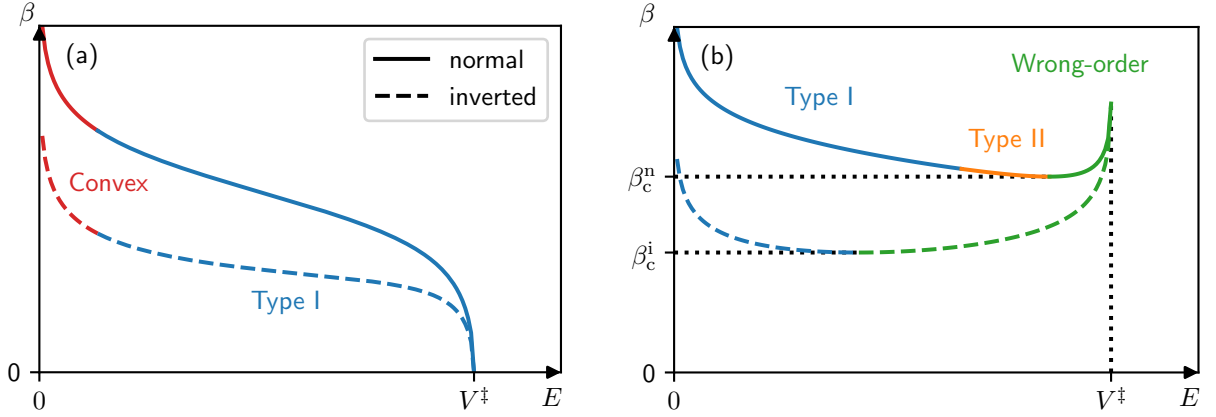


Figure 2: Illustration of inverse temperature β (imaginary time) of (a) simple instantons (upper path in Figure 1b) and (b) concerted instantons (lower path in Figure 1b) as a function of tunneling energy E . The solid line is for the normal regime and the dashed line is for the inverted regime. Both regimes have the same crossover point. The crossing point energy V^\ddagger and the crossover inverse temperature β_c of concerted instantons for each case are marked on the axes. β_c corresponds to the highest temperature where a concerted instanton can exist, and the superscripts n and i stand for the normal and inverted regimes respectively. The wrong-order instantons have an overall minus sign in their prefactors, leading to unphysical imaginary rates.

based on the nature of their tunneling mechanism, which divides them into “simple” and “concerted” types. Specifically, concerted instantons simultaneously traverse a diabatic barrier and switch electronic state (lower nonadiabatic instanton in Figure 1b), while the simple instanton does not cross a diabatic barrier (upper nonadiabatic instanton in Figure 1b). The simple instanton is always type I regardless of its energy E (Figure 2a), and shares many similarities with a convex-regime instanton. For example, as the temperature increases, it continuously collapses towards the MECP. Meanwhile, as the temperature decreases, it may even transition to a convex instanton (Figure 2a), for the reason that the majority of the instanton imaginary time is spent near the minimum rather than the barrier. Concerted instantons, however, exhibit distinct behavior. At low temperatures, they are type I. As the temperature increases, in the normal regime, they transition to type II instantons, while in the inverted regime, type II instantons are not found (Figure 2b). A key feature of concerted instantons is that they only exist below a certain temperature (we refer to it as the crossover

temperature T_c), which is a property normally only found for adiabatic instantons. Note that it is difficult to predict T_c for the concerted instanton, since unlike adiabatic instantons, it is not simply determined by the imaginary frequency at the barrier top. Nevertheless, we find that it is typically higher than the T_c of an adiabatic instanton on the diabatic barrier on V_0 . This is because the barrier formed by crossing PESs is narrower than the diabatic barrier (Figure 1b), making it easier for an instanton to exist. The unusual appearance of T_c in nonadiabatic instantons arises from the concerted instanton traversing a rounded barrier on a diabatic PES, similar to a Born–Oppenheimer instanton. In contrast, convex instantons exist at any temperature.

Another key feature is that as the energy E of a concerted instanton increases, it undergoes a transition from a type I (or type II if it exists) to a wrong-order instanton (Figure 2b)[†]. The wrong-order instanton has an extra negative eigenvalue in the prefactors, resulting in an imaginary instanton partition function. We note that identical behavior has been previously discovered in adiabatic instantons on a broad-top barrier.⁴⁹ The wrong-order instanton cannot be directly used to compute canonical rates, as Eq. (12) will give an unphysical imaginary rate constant.

3.2 Analytic continuation

The sign changes observed in various terms of the SCI prefactor in the non-convex regime may appear problematic. However, Eq. (12) remains well-defined even if we relax the sign constraints on the individual prefactor terms imposed by the derivation, since the rate should always be real, which can be satisfied if the prefactors are treated in this way. This motivates an analytic continuation from the convex to the non-convex regime. We propose an analytic continuation scheme via the deformation of the potential to cover all types of non-convex-regime instantons mentioned above.

A natural next step is to bridge the two regimes by continuously deforming a pair of

[†]Type II was not found for the inverted regime likely due to the wrong-order instanton appearing before a type-II instanton could exist.

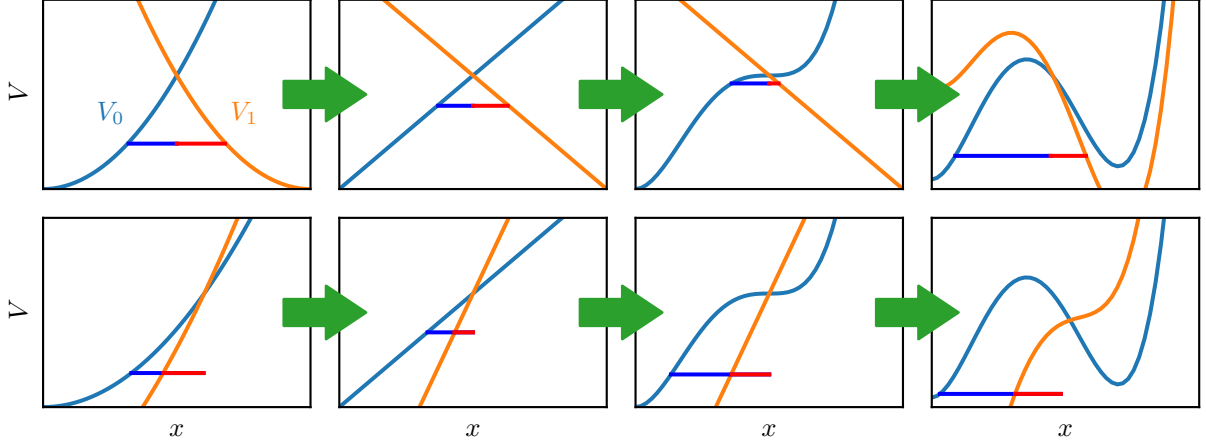


Figure 3: Illustration of an analytic continuation scheme from a convex regime instanton to a non-convex regime instanton. The tunneling paths on either state (in blue and red) form the instantons. The top row is for the normal regime, and the bottom row is for the inverted regime. From left to right, we deform the potentials from a 1D convex model to a linear model, and then introduce negative curvature in V_0 and V_1 .

crossing convex potentials into two non-convex surfaces (Figure 3). It is well established that instanton theory performs very well in both the normal and inverted regimes of convex systems, such as those illustrated in the first column of Figure 3).²⁶ Then for any given non-convex instanton at a near-barrier crossing (e.g., the final column in Figure 3), one can construct a continuous deformation of the PESs such that the instanton smoothly evolves from the convex regime to the target non-convex configuration.

Instanton theory can be analytically continued using the aforementioned procedure, provided that no singularities occur in the prefactors during the surface reshaping. A potentially problematic case arises in systems with linear potentials, where $C \rightarrow 0$ and $\frac{d^2 S}{d\tau^2} \rightarrow \infty$.²¹ However, as shown in Ref. 21, the instanton rate remains well-defined and, in fact, exactly reproduces FGR for linear potentials. In this case, the singularity in $\frac{d^2 S}{d\tau^2}$ cancels with the vanishing C , yielding a finite result. Equivalently, one finds that Σ remains well-defined. Now we have successfully justified the analytical continuation from a convex instanton to a type I one through a linear system for both the normal and inverted regimes.

Next we are to resolve the singularity caused by a conjugate point, which is related to

the analytic continuation from type I to type II. It can be proven that the singularity of C_n also cancels with that of Σ in this case since their singularities are caused by the same term in the same order (proof given in SI Section S2). It is now safe to carry out the analytic continuation throughout the entire surface deformation process, as no singularities exist to obstruct it. Specifically, the prefactor can be calculated using $\sqrt{\frac{C_0 C_1}{-\Sigma}}$ instead of the potentially ill-defined expression $\frac{\sqrt{C_0} \sqrt{C_1}}{\sqrt{-\Sigma}}$.

Finally, we present additional evidence supporting the validity of the analytically continued instanton rate expression in the non-convex regime. Firstly, in the classical limit, the instanton rate correctly reduces to the NA-TST rate in the non-convex regime (proof given in Appendix A). Secondly, we provide a direct first-principles derivation of instanton theory in the Hamilton–Jacobi formalism,²¹ based on Green’s functions instead of propagators for the non-convex normal regime. In particular, we prove in SI Section S3 that Green’s functions remain well behaved even in situations where propagators become problematic, and for all systems tested thus far, the resulting prefactors are consistently positive, thereby justifying the steepest-descent integration. Although this derivation does not extend naturally to the inverted regime, where Green’s functions become highly oscillatory and lack a well-defined peak,²⁶ it provides further independent support for our analytic continuation approach.

4 Numerical results

4.1 Benchmarking extended instanton theory in model systems

In this section, we benchmark our extended instanton theory using a one-dimensional model system composed of an asymmetric double well intersected by a linear potential, defined by

$$V_0 = \lambda \left(\frac{x}{\xi} + 1 \right)^2 \left(\frac{x}{\xi} - 1 \right)^2 + \kappa_0 x + \varepsilon_0, \quad (14a)$$

$$V_1 = \kappa_1 x + \varepsilon_1, \quad (14b)$$

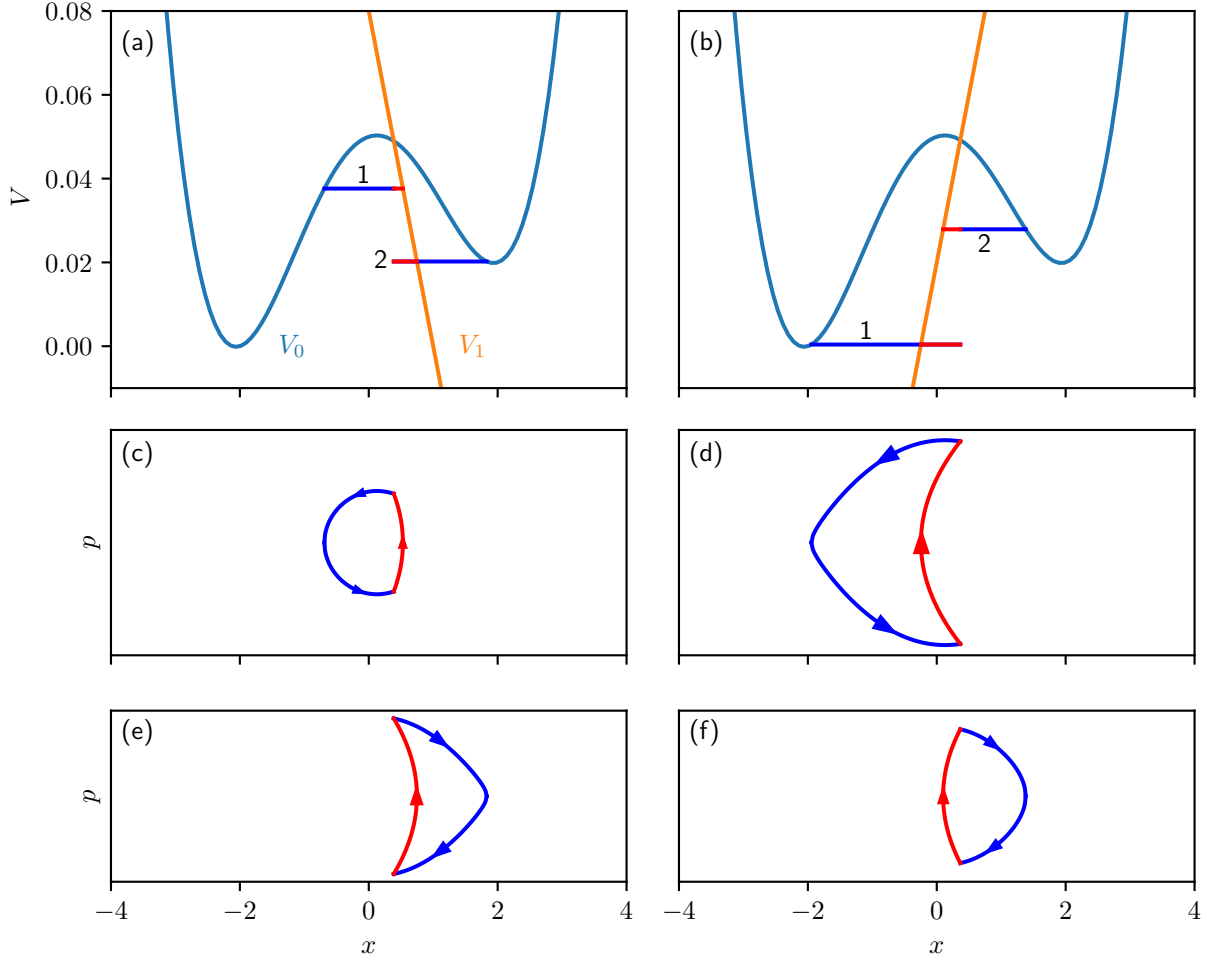


Figure 4: Diabatic potentials defined in Eq. (14), where the instanton describing concerted tunneling is in the normal regime for model A (a) and in the inverted regime for model B (b). All instantons displayed are optimized at $\beta = 1000$. Panels c-f show the instantons in phase space. (c) The type-II normal regime. (d) The type-I inverted regime. (e) The convex inverted regime. (f) The type-I normal regime. Note that there is no fundamental difference in the shapes of the convex and non-convex instantons in phase space. The key distinction lies between the normal and inverted regimes.

with $m = 1836$, $\lambda = 0.04$, $\xi = 2$, $\kappa_0 = 0.005$, $\varepsilon_0 = 0.01$ and $\Delta = 0.0004$ given in atomic units. We test two parameter sets for κ_1 and ε_1 to cover both the non-convex normal and inverted regime, as shown in Figure 4. We set $\kappa_1 = -0.08$, $\varepsilon_1 = 0.08$ for the normal-regime model A, and $\kappa_1 = 0.08$, $\varepsilon_1 = 0.02$ for the inverted-regime model B. Figure 4 illustrates the model potentials along with two optimized nonadiabatic instantons at $\beta = 1000$ for each model, where the concerted instanton is labeled as 1 and the simple instanton is labeled as

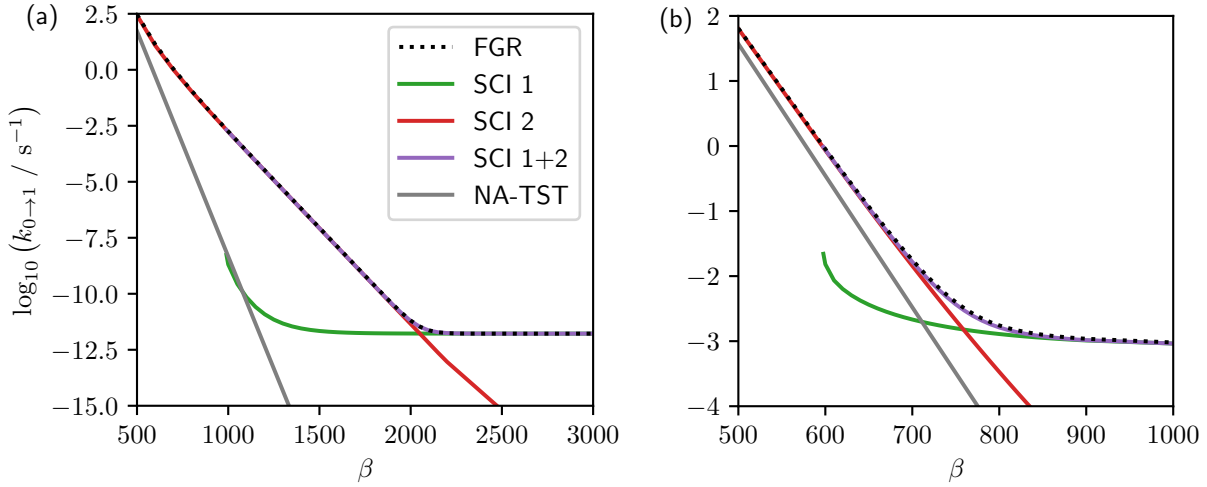


Figure 5: Rate constants for the reaction from state 0 to state 1 $k_{0 \rightarrow 1}$ as a function of inverse temperature β for model A (a) and model B (b). For FGR, the exact reactant partition function is used, while the remaining methods employ the harmonic approximation to Z_0 evaluated at the minimum of the left well.

2.

In Figure 5, we present the rate constants for the transitions from state 0 to state 1 in both models, computed with SCI, NA-TST and, for comparison, FGR. In the FGR calculations, we use the exact reactant partition function Z_0 , obtained by summing the Boltzmann factors associated with the vibrational eigenstates of the reactant potential. Instead, the SCI and NA-TST calculations evaluate Z_0 based on a harmonic approximation around the minimum of the left well, even for instanton 2, which describes transitions starting from the right well (see Figure 4). The reason is that this yields a rate k_2 equivalent to the pre-equilibrium approximation, which assumes rapid equilibration between the left and right wells before the electronic state transition, and makes it directly comparable to k_1 from instanton 1 and the FGR rate. Figure 5 highlights the excellent agreement between the FGR rate and the SCI rate, with the latter obtained as the sum of contributions from instantons 1 and 2. The maximum relative error is only 4% for the first model and 7% for the second.

As expected, the simple instanton dominates at high temperatures, where it approaches the NA-TST rate, and instanton 1 ceases to exist above the crossover temperature. At low

temperatures, however, this situation changes dramatically, with the concerted instanton 1 becoming dominant. This is because at low temperature, only the lowest energy levels in the left well are significantly populated. These asymptotic trends confirm that instanton 1 is a purely quantum-mechanical deep-tunneling path, while instanton 2 transitions smoothly from deep to shallow tunneling, and ultimately to the classical limit.

4.2 Nonadiabatic tunneling mechanisms in the non-convex regime

In practice, we are often interested in the overall rate, which refers to the rate of escaping from a well on the reactant state and reaching a specific minimum on the product state, such as the process from R_0 to P_1 as depicted in Figure 1. There are two available mechanisms for such a process, with one being sequential and the other being concerted. The sequential mechanism, where the system first crosses the diabatic barrier on V_0 and subsequently undergoes a nonadiabatic transition to V_1 via instanton 2 in Figure 4, was previously thought to be the only pathway for the overall reaction.¹⁵ In the high-temperature limit, the tunneling rate associated with this mechanism reduces to its classical counterpart. In contrast, the concerted mechanism, in which both processes occur concomitantly, represents a deep-tunneling pathway with no classical analogue. In the following we demonstrate that this purely quantum-mechanical pathway can in fact dominate over the sequential mechanism at low temperatures.

The evaluation of the overall reaction rate for the sequential mechanism involves both the adiabatic rate on the reactant state and the non-adiabatic rate for hopping from the reactant state to the product state. The rate constant for the adiabatic step, traversing the diabatic barrier without a change in electronic state, denoted as step 3, can be accurately described by Born–Oppenheimer instanton theory.⁵⁰ The concerted rate k_{con} is exactly the same as k_1 , while the sequential rate is a combination of steps 2 and 3, given by

$$k_{\text{seq}} = \frac{k_2}{2k_{-3}} \left(k_3 - k_{-3} - k_2 + \sqrt{(k_3 - k_{-3} - k_2)^2 + 4k_3k_{-3}} \right), \quad (15)$$

where k_{-3} is the rate constant of the reverse reaction of step 3, and, in contrast to the previous subsection, k_2 is calculated with Z_0 evaluated in the right well. Eq.(15) is derived by analytically solving the rate equations under an infinite sink approximation on the product side to obtain the time-dependent rate $k(t)$, and then taking the limit as $t \rightarrow +\infty$ (see Appendix B for derivation). If $k_2 \gg \{k_3, k_{-3}\}$, the overall rate k_{seq} reduces to the rate-determining step k_3 . Conversely, if $k_2 \ll \{k_3, k_{-3}\}$, the rate-determining step becomes k_2 , and k_{seq} reduces to the pre-equilibrium approximation $k_2 \frac{k_3}{k_{-3}}$.

We explore the competition between sequential and concerted mechanisms by studying models A and B from the previous subsection (see Figure 4) across a range of different parameters. The relative importance of the two mechanisms depends on several factors, including the potential-energy difference between the reactant wells, the nonadiabatic coupling, the distance between the TS and the MECP, the length of the reaction path, and the barrier height. Here, we focus on the effect of the energy difference between the reactant wells, which is controlled by κ_0 (Figure 6), while keeping all other parameters fixed as defined in

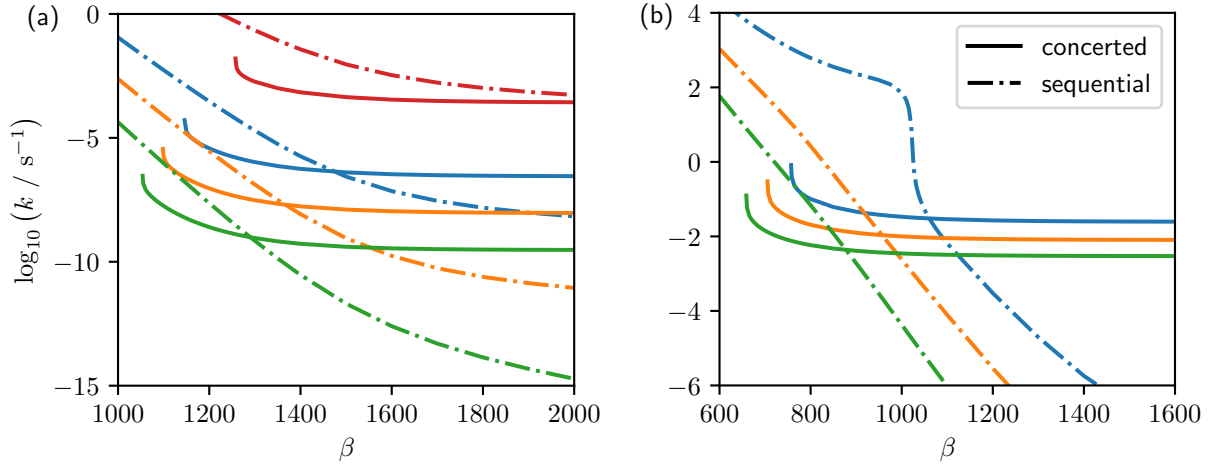


Figure 6: Overall rate constants k for the sequential and concerted mechanisms in model A (a) and model B (b) as functions of inverse temperature β . Each color corresponds to a different value of κ_0 : red for $\kappa_0 = -0.006$, blue for $\kappa_0 = -0.002$, orange for $\kappa_0 = 0$ and green for $\kappa_0 = 0.002$. Solid and dashed-dotted lines of the same color represent the concerted and sequential contributions, respectively.

Section S4 of the SI. Since the potentials used here qualitatively mimic the typical reaction paths at near-barrier crossings, we expect the qualitative trends to carry over to more complex molecular systems. In fact, the theoretical framework in this paper has recently been used to explore the concerted tunneling pathway in carbenes, where the potential energy profiles are rather similar to the model used here.²⁹

In Figure 6, we consider exothermic ($\kappa_0 < 0$), symmetric ($\kappa_0 = 0$) and endothermic ($\kappa_0 > 0$) adiabatic reaction steps. In all cases except for the most exothermic variant of model A ($\kappa_0 = -0.006$, red lines in Figure 6a), a crossover occurs between the rates of the sequential and the concerted mechanisms. As expected from the results in Section 4.1, the sequential mechanism dominates at high temperatures, while the concerted mechanism governs the low-temperature regime. It can be seen that the temperature at which the two rates coincide decreases with growing endothermicity of the adiabatic reaction step, i.e., the concerted mechanism dominates already at higher temperatures. For $\kappa_0 = -0.006$, the crossing point is at a far lower temperature and even beyond the shown temperature range. This can be explained by the fact that a more negative κ_0 leads to not only a more exothermic reaction but also a narrower barrier. Therefore, the adiabatic instanton, determining k_{seq} , is shorter than its original length, with a reduction approximately twice that of the concerted instanton, since the other end of the concerted instanton is on V_1 , which is fixed here. Note that the sequential mechanism can be faster than the concerted one at all temperatures, provided that both k_1 and k_3 converge as $\beta \rightarrow \infty$, with the former’s limit dependent of nonadiabatic coupling and the latter’s limit independent of it. As κ_0 is varied from negative to positive in model A, k_{seq} decreases much more rapidly at low temperatures. The reason is that, for $\kappa_0 \leq 0$, the instanton energy approaches the minimum of the left well, corresponding to a tunneling process from the bottom of the well, which yields a finite rate constant in the low-temperature limit. In contrast, for $\kappa_0 > 0$, the instanton energy is bounded from below by the minimum of the right well, and thus the reaction always requires an initial thermal activation. This results in an exponential suppression of the rate

constant as $\beta \rightarrow \infty$.

Model B exhibits similar trends for the competition between the two mechanisms. However, while in model A, $k_{\text{seq}} \approx k_3$, model B requires the usage of Eq. (15) because the rate constants entering the formula for the sequential rate are now comparable in magnitude. As the temperature decreases, the dominant contribution to k_{seq} shifts from $k_2 \frac{k_3}{k_{-3}}$ to k_3 , reflecting a change in the rate-determining step from k_2 to k_3 . This transition is especially pronounced for $\kappa_0 = -0.002$ (dashed-dotted blue curve in Figure 6b), where a sharp drop in the rate occurs around $\beta = 1000$. The origin of this behavior is that $k_3 \gg k_{-3}$ for this parameter set. In that regime, when k_2 becomes comparable to k_3 , the term $k_2 \frac{k_3}{k_{-3}}$ grows much larger than k_3 , resulting in a sudden decrease in k_{seq} as it transitions from being governed by $k_2 \frac{k_3}{k_{-3}}$ to being limited by k_3 alone. This illustrates the rich interplay between different reaction steps that can emerge from varying a single parameter, and underscores the importance of capturing competing nuclear quantum effects in non-convex molecular systems in their full complexity, as is made possible by our extended instanton theory.

We have also investigated intersecting double-well models similar to the one shown in Figure 1b. As demonstrated in SI Section S4, these models exhibit no qualitative differences from our models A and B, which is why we have focused our analysis on those two representative cases.

5 Conclusions

We have developed an extended semiclassical instanton theory capable of describing nonadiabatic tunneling in systems where an electronic-state crossing occurs near a diabatic barrier. Unlike previous instanton formulations that assumed mostly convex diabatic potentials, the present approach generalizes SCI to this non-convex regime, where tunneling paths may traverse large regions of negative curvature. The fluctuation factors of the non-convex instantons exhibit different signs than their convex counterparts due to the occurrence of con-

jugate points along the paths, which appear to invalidate the theory. We resolve this issue by analytically continuing the instanton rate expression to the non-convex regime. Benchmark comparisons to other methods for model systems demonstrate that the extended instanton theory yields excellent agreement with fully quantum-mechanical FGR rates across a wide range of parameters, including in the deep-tunneling regime, and reduces to NA-TST in the classical limit.

It is particularly interesting that the non-convex instanton theory enables the study of the competition between a sequential reaction mechanism, and a deep-tunneling concerted mechanism without classical analogue. Previously, only the sequential mechanism involving an intermediate adiabatic step followed by a nonadiabatic transition has been considered. While this reaction path prevails at high temperatures, we show that the concerted mechanism can dominate at low temperatures. The interplay between the two mechanisms strongly depends on a multitude of factors, such as the potential energy asymmetry, nonadiabatic coupling strength, and barrier shape. A rich dynamical behavior is thus observed, emphasizing the need for a unified framework, as provided by our extended instanton theory, that captures the full complexity of nonadiabatic quantum tunneling in molecular systems.

Although our analysis focused on simplified one-dimensional models, the qualitative trends identified here are expected to generalize to multidimensional molecular systems. In addition, our extended instanton theory provides a computationally efficient and quantitatively accurate tool for studying competing sequential and concerted nonadiabatic tunneling in molecular systems with near-barrier crossings. This has recently been demonstrated in Ref. 29, where one of the instantons discussed here was used to explain the temperature-dependent selectivity observed in spin crossovers of carbenes.

Acknowledgement

Z.Y. and W.F. are supported by the National Natural Science Foundation of China under Grant No. 22321003. E.R.H is grateful for financial support from the Swiss National Science Foundation through Grant 214242. J.O.R. acknowledges financial support from the Swiss National Science Foundation through Project 207772.

Supporting Information Available

Additional details, including some derivations and further numerical test data, are provided in the Supporting Information.

Appendix A Classical limit

As shown in SI Section S1, an extra minus may arise in C_n due to the existence of a conjugate point. However, in the classical limit, C_n will never encounter this problem, since the conjugate point can only exist when a trajectory is long enough. However, we will show that \mathbf{C} may have negative eigenvalues in the classical limit of the non-convex regime.

The classical short-time limit of the action takes the form of²²

$$S_n = \frac{m \|x_-\|^2}{2z_n} + V_n(x_+) z_n, \quad (\text{A1})$$

where $x_+ = \frac{1}{2}(x' + x'')$, $x_- = x' - x''$, and \mathbf{C} is block-diagonal with entries

$$\frac{\partial^2 S}{\partial x_+ \partial x_+} = \beta \hbar \widetilde{\mathbf{H}}, \quad (\text{A2})$$

$$\frac{\partial^2 S}{\partial x_- \partial x_-} = \frac{m\beta\hbar}{\tau_0\tau_1} \mathbf{I}_f, \quad (\text{A3})$$

where $\widetilde{\mathbf{H}} \equiv \frac{1}{\beta\hbar} (\tau_0 \mathbf{H}_0 + \tau_1 \mathbf{H}_1)$, and \mathbf{I}_f is an $f \times f$ identity matrix. Similar to the 1D system,

the sign of Eq. (A3) indicates whether it is in the normal or inverted regime, and Eq. (A2) gives a positive definite matrix as long as both \mathbf{H}_0 and \mathbf{H}_1 are positive definite. If an imaginary frequency exists in either \mathbf{H}_0 or \mathbf{H}_1 , may also appear in $\widetilde{\mathbf{H}}$, and hence in $\frac{\partial^2 S}{\partial x_+ \partial x_+}$.

However, it can be proven that instanton theory does not break down in the classical limit even if the positive-definiteness of \mathbf{C} is not satisfied. Inserting Eq. (A1) into Eq. (6), we obtain

$$k_{\text{cl}} Z_0 = \frac{1}{\hbar^2 (2\pi\hbar)^f} \iiint |\Delta(x_+)|^2 \left(\frac{m}{\sqrt{z_0 z_1}} \right)^f e^{-\frac{m\beta}{2z_0 z_1} \|x_-\|^2 - \frac{1}{\hbar} [V_0(x_+)z_0 + V_1(x_+)z_1]} dx_- dx_+ dt, \quad (\text{A4})$$

and x_- can be easily integrated out analytically to give

$$k_{\text{cl}} Z_0 = \frac{1}{\hbar^2} \left(\frac{m}{2\pi\beta\hbar^2} \right)^{f/2} \iint |\Delta(x_+)|^2 e^{-\frac{1}{\hbar} [V_0(x_+)z_0 + V_1(x_+)z_1]} dx_+ dt. \quad (\text{A5})$$

Next, we would integrate Eq. (A5) over x_+ first and then t if we follow the previous derivation of instanton theory. However, the potential non-positive-definiteness of Eq. (A2) may prevent us from doing so. Nevertheless, we can alternatively integrate Eq. (A5) over t first by Fourier transform to give

$$k_{\text{cl}} Z_0 = \frac{2\pi}{\hbar} \left(\frac{m}{2\pi\beta\hbar^2} \right)^{f/2} \int |\Delta(x_+)|^2 e^{-\beta\widetilde{V}(x_+)} \delta[V_0(x_+) - V_1(x_+)] dx_+, \quad (\text{A6})$$

where $\widetilde{V} \equiv \frac{1}{\beta\hbar} (\tau_0 V_0 + \tau_1 V_1)$. After steepest-descent approximation applied to Eq. (A6), the commonly used classical golden-rule rate is reproduced as

$$k_{\text{cl}} Z_0 = \sqrt{\frac{2\pi m}{\beta\hbar^2}} \frac{\Delta^2}{\hbar |\mathbf{g}_0^\dagger - \mathbf{g}_1^\dagger|} Z^\dagger e^{-\beta V^\dagger}, \quad (\text{A7})$$

$$Z^\dagger = \prod_{i=1}^{f-1} \frac{1}{\beta\hbar\widetilde{\omega}_i}, \quad (\text{A8})$$

where \mathbf{g}_n^\dagger are gradients, $\widetilde{\omega}_i$ are vibrational frequencies obtained by diagonalizing $\widetilde{\mathbf{H}}$ excluding

the reaction coordinate, and all quantities are evaluated at the MECP.

We find from the derivation above that starting from Eq. (A4), the only approximation we make is the steepest-descent approximation, requiring all $\tilde{\omega}_i$ (other than the frequency in the direction of the reaction coordinate) to be real. This condition can always be satisfied since it is also the necessary condition for a point to be MECP, and the imaginary frequencies (if any), typically associated with the reaction coordinates, i.e., the gradients, will always be projected out. Therefore, instanton theory can always lead to the correct classical rate, regardless of the definiteness of $\widetilde{\mathbf{H}}$.

Appendix B Derivation of the overall reaction rate

Consider a multi-step reaction network system as illustrated in Figure 7. The reaction kinetics can be described using the law of mass action as

$$\frac{d[\mathbf{R}]}{dt} = -(k_1 + k_3) [\mathbf{R}] + k_{-3} [\mathbf{I}], \quad (\text{B1})$$

$$\frac{d[\mathbf{I}]}{dt} = k_3 [\mathbf{R}] - (k_2 + k_{-3}) [\mathbf{I}], \quad (\text{B2})$$

$$\frac{d[\mathbf{P}]}{dt} = k_1 [\mathbf{R}] + k_2 [\mathbf{I}], \quad (\text{B3})$$

where square brackets denote concentrations, and the infinite sink approximation is applied to P, thereby neglecting reactions originating from P. Given boundary conditions $[\mathbf{R}]_{t=0} = [\mathbf{R}]_0$ and $[\mathbf{I}]_{t=0} = 0$, the solutions of Eq. (B1) and (B2) are

$$[\mathbf{R}] = \frac{[\mathbf{R}]_0}{\sqrt{A}} \left(-\rho_- e^{r_+ t} + \rho_+ e^{r_- t} \right), \quad (\text{B4})$$

$$[\mathbf{I}] = \frac{[\mathbf{R}]_0}{\sqrt{A}} k_3 \left(-e^{r_+ t} + e^{r_- t} \right), \quad (\text{B5})$$

where $A = (k_1 - k_2 + k_3 - k_{-3})^2 + 4k_3k_{-3}$, $r_{\pm} = \frac{1}{2} \left(-(k_1 + k_2 + k_3 + k_{-3}) \pm \sqrt{A} \right)$, and $\rho_{\pm} = r_{\pm} + k_1 + k_3$. Inserting Eq. (B4) and (B5) into Eq. (B3), we obtain the time evolution

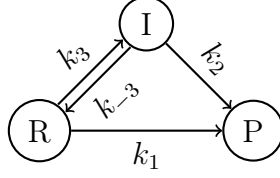


Figure 7: A schematic reaction network illustrating the systems in Figure 4. There are two pathways leading from the reactant (R) to the product (P), with one path being direct and the other through an intermediate species (I).

of the overall rate as

$$\frac{d[P]}{dt} = \frac{[R]_0}{\sqrt{A}} \left(k_2 k_3 \left(-e^{r+t} + e^{r-t} \right) + k_1 \left(-\rho_- e^{r+t} + \rho_+ e^{r-t} \right) \right). \quad (B6)$$

The time-dependent overall rate constant is defined by

$$k(t) \equiv \frac{1}{[R]} \frac{d[P]}{dt}. \quad (B7)$$

Therefore, we find the analytical expression of $k(t)$, which is

$$k(t) = k_1 + k_2 k_3 \frac{-e^{r+t} + e^{r-t}}{-\rho_- e^{r+t} + \rho_+ e^{r-t}}. \quad (B8)$$

By taking the limit $t \rightarrow +\infty$ to Eq. (B8), the resulting overall rate constant is obtained as

$$k_{\text{overall}} \equiv \lim_{t \rightarrow +\infty} k(t) \quad (B9)$$

$$= k_1 + \frac{k_2 k_3}{\rho_-} \quad (B10)$$

$$= k_1 + \frac{k_2}{2k_{-3}} \left(k_1 - k_2 + k_3 - k_{-3} + \sqrt{(k_1 - k_2 + k_3 - k_{-3})^2 + 4k_3 k_{-3}} \right), \quad (B11)$$

and the sequential rate constant can be obtained by setting k_1 as zero in Eq. (B11), giving

$$k_{\text{seq}} = \frac{k_2}{2k_{-3}} \left(k_3 - k_{-3} - k_2 + \sqrt{(k_3 - k_{-3} - k_2)^2 + 4k_3 k_{-3}} \right). \quad (B12)$$

References

- (1) González, L.; Lindh, R. *Quantum Chemistry and Dynamics of Excited States: Methods and Applications*; Wiley: Hoboken, NJ, 2021.
- (2) Harvey, J. N. Spin-forbidden reactions: Computational insight into mechanisms and kinetics. *Wiley Interdiscip. Rev.: Comput. Mol. Sci.* **2014**, *4*, 1–14.
- (3) Brookes, J. C. Quantum effects in biology: Golden rule in enzymes, olfaction, photosynthesis and magnetodetection. *Proc. R. Soc. A* **2017**, *473*, 20160822.
- (4) Yarkony, D. R. Nonadiabatic quantum chemistry—Past, present, and future. *Chem. Rev.* **2012**, *112*, 481–498.
- (5) Butler, L. J. Chemical reaction dynamics beyond the Born-Oppenheimer approximation. *Annu. Rev. Phys. Chem.* **1998**, *49*, 125–171.
- (6) Zwanzig, R. *Nonequilibrium Statistical Mechanics*; Oxford University Press: Oxford ; New York, 2001; pp 48–53.
- (7) Ulstrup, J. *Charge Transfer Processes in Condensed Media*; Springer-Verlag: Berlin, 1979.
- (8) Jortner, J. Radiationless transitions. *Pure and Applied Chemistry* **1971**, *27*, 389–419.
- (9) Marcus, R. A. On the theory of oxidation-reduction reactions involving electron transfer. I. *J. Chem. Phys.* **1956**, *24*, 966–978.
- (10) Marcus, R. A. Exchange reactions and electron transfer reactions including isotopic exchange. Theory of oxidation-reduction reactions involving electron transfer. Part 4.—A statistical-mechanical basis for treating contributions from solvent, ligands, and inert salt. *Discuss. Faraday Soc.* **1960**, *29*, 21–31.

- (11) Marcus, R. A.; Sutin, N. Electron transfers in chemistry and biology. *Biochim. Biophys. Acta* **1985**, *811*, 265–322.
- (12) Lorquet, J. C.; Leyh-Nihant, B. Nonadiabatic unimolecular reactions. 1. A statistical formulation for the rate constants. *J. Phys. Chem.* **1988**, *92*, 4778–4783.
- (13) Cui, Q.; Morokuma, K.; Bowman, J. M.; Klippenstein, S. J. The spin-forbidden reaction $\text{CH}(^2\Pi) + \text{N}_2 \rightarrow \text{HCN} + \text{N}(^4S)$ revisited. II. Nonadiabatic transition state theory and application. *J. Chem. Phys.* **1999**, *110*, 9469–9482.
- (14) Harvey, J. N.; Aschi, M. Spin-forbidden dehydrogenation of methoxy cation: A statistical view. *Phys. Chem. Chem. Phys.* **1999**, *1*, 5555–5563.
- (15) Harvey, J. N. Spin-forbidden reactions: Computational insight into mechanisms and kinetics. *WIREs Comput. Mol. Sci.* **2014**, *4*, 1–14.
- (16) Delos, J. B. On the reactions of N_2 with O. *J. Chem. Phys.* **1973**, *59*, 2365–2369.
- (17) Lykhin, A. O.; Kaliakin, D. S.; dePolo, G. E.; Kuzubov, A. A.; Varganov, S. A. Nonadiabatic transition state theory: Application to intersystem crossings in the active sites of metal-sulfur proteins. *Int. J. Quantum Chem.* **2016**, *116*, 750–761.
- (18) Heller, E. R.; Richardson, J. O. Spin crossover of thiophosgene via multidimensional heavy-atom quantum tunneling. *J. Am. Chem. Soc.* **2021**, *143*, 20952–20961.
- (19) Heller, E. R.; Richardson, J. O. Heavy-atom quantum tunnelling in spin crossovers of nitrenes. *Angew. Chem., Int. Ed. Engl.* **2022**, *61*, e202206314.
- (20) Miller, W. H. Semiclassical limit of quantum mechanical transition state theory for nonseparable systems. *J. Chem. Phys.* **1975**, *62*, 1899–1906.
- (21) Richardson, J. O.; Bauer, R.; Thoss, M. Semiclassical Green’s functions and an instanton formulation of electron-transfer rates in the nonadiabatic limit. *J. Chem. Phys.* **2015**, *143*, 134115.

- (22) Richardson, J. O. Ring-polymer instanton theory of electron transfer in the nonadiabatic limit. *J. Chem. Phys.* **2015**, *143*, 134116.
- (23) Ansari, I. M.; Heller, E. R.; Trenins, G.; Richardson, J. O. Instanton theory for Fermi’s golden rule and beyond. *Philos Trans A Math Phys Eng Sci* **2022**, *380*, 20200378.
- (24) Richardson, J. O. Nonadiabatic tunneling in chemical reactions. *J. Phys. Chem. Lett.* **2024**, *15*, 7387–7397.
- (25) Feynman, R. P.; Hibbs, A. R. *Quantum Mechanics and Path Integrals*, 20th ed.; International Series in Pure and Applied Physics; McGraw-Hill: New York, NY, 1995.
- (26) Heller, E. R.; Richardson, J. O. Instanton formulation of Fermi’s golden rule in the Marcus inverted regime. *J. Chem. Phys.* **2020**, *152*, 034106.
- (27) Fang, W.; Heller, E. R.; Richardson, J. O. Competing quantum effects in heavy-atom tunnelling through conical intersections. *Chem. Sci.* **2023**, *14*, 10777–10785.
- (28) Ansari, I. M.; Heller, E. R.; Trenins, G.; Richardson, J. O. Heavy-atom tunnelling in singlet oxygen deactivation predicted by instanton theory with branch-point singularities. *Nat. Commun.* **2024**, *15*, 4335.
- (29) Manae, M. A.; Richardson, J. O. Temperature-dependent mechanistic control of nonadiabatic tunnelling in triplet carbenes. *Angew. Chem., Int. Ed.* **2025**, e202503066.
- (30) Gagliardi, C. J.; Westlake, B. C.; Kent, C. A.; Paul, J. J.; Papanikolas, J. M.; Meyer, T. J. Integrating proton coupled electron transfer (PCET) and excited states. *Coord. Chem. Rev.* **2010**, *254*, 2459–2471.
- (31) Zhu, Q.; Soudackov, A. V.; Tommos, C.; Hammes-Schiffer, S. Proton-coupled electron transfer upon oxidation of tyrosine in a de novo protein: Analysis of proton acceptor candidates. *Biochemistry* **2024**, *63*, 1999–2008.

- (32) Hutchison, P.; Soudackov, A. V.; Hammes-Schiffer, S. Nonadiabatic proton-coupled electron transfer at a graphitic surface immobilized cobalt porphyrin. *ACS Catal.* **2024**, *14*, 14363–14372.
- (33) Pharr, C. R.; Esselman, B. J.; McMahon, R. J. Photochemistry of 1-(2- and 3-thienyl)diazoethanes: Spectroscopy and tunneling reaction of triplet 1-(3-thienyl)ethyldiene. *J. Org. Chem.* **2023**, *88*, 16176–16185.
- (34) Besora, M.; Harvey, J. N. Understanding the rate of spin-forbidden thermolysis of HN_3 and CH_3N_3 . *J. Chem. Phys.* **2008**, *129*, 044303.
- (35) Nunes, C. M.; Viegas, L. P.; Wood, S. A.; Roque, J. P. L.; McMahon, R. J.; Fausto, R. Heavy-atom tunneling through crossing potential energy surfaces: Cyclization of a triplet 2-formylarylnitrene to a singlet 2,1-benzisoxazole. *Angew. Chem., Int. Ed.* **2020**, *59*, 17622–17627.
- (36) Li, X.; Lu, B.; Jiang, J.; Wang, L.; Trabelsi, T.; Francisco, J. S.; Fang, W.; Zhou, M.; Zeng, X. Water complex of imidogen. *J. Am. Chem. Soc.* **2023**, *145*, 1982–1987.
- (37) Viegas, L. P.; M. Nunes, C.; Fausto, R. Spin-forbidden heavy-atom tunneling in the ring-closure of triplet cyclopentane-1,3-diyl. *Phys. Chem. Chem. Phys.* **2021**, *23*, 5797–5803.
- (38) Johansson, A. J.; Blomberg, M. R. A.; Siegbahn, P. E. M. Quantum chemical modeling of the oxidation of dihydroanthracene by the biomimetic nonheme iron catalyst $[(\text{TMC})\text{Fe}^{\text{IV}}(\text{O})]^{2+}$. *J. Phys. Chem. C* **2007**, *111*, 12397–12406.
- (39) Usharani, D.; Janardanan, D.; Li, C.; Shaik, S. A theory for bioinorganic chemical reactivity of oxometal complexes and analogous oxidants: The exchange and orbital-selection rules. *Acc. Chem. Res.* **2013**, *46*, 471–482.

- (40) Canale, V.; Robinson, J. R.; Zavras, A.; Khairallah, G. N.; d'Alessandro, N.; Yates, B. F.; O'Hair, R. A. Two spin-state reactivity in the activation and cleavage of CO₂ by [ReO₂]⁻. *J. Phys. Chem. Lett.* **2016**, 7, 1934–8.
- (41) Zhou, S.; Li, J.; Firouzbakht, M.; Schlangen, M.; Schwarz, H. Sequential gas-phase activation of carbon dioxide and methane by [Re(CO)₂]⁺: The sequence of events matters! *J. Am. Chem. Soc.* **2017**, 139, 6169–6176.
- (42) Dergachev, I. D.; Dergachev, V. D.; Rooein, M.; Mirzanejad, A.; Varganov, S. A. Predicting kinetics and dynamics of spin-dependent processes. *Acc. Chem. Res.* **2023**, 56, 856–866.
- (43) Miller, W. H.; Schwartz, S. D.; Tromp, J. W. Quantum mechanical rate constants for bimolecular reactions. *J. Chem. Phys.* **1983**, 79, 4889–4898.
- (44) Wolynes, P. G. Imaginary time path integral Monte Carlo route to rate coefficients for nonadiabatic barrier crossing. *J. Chem. Phys.* **1987**, 87, 6559–6561.
- (45) Chandler, D. In *Classical and Quantum Dynamics in Condensed Phase Simulations*; Berne, B. J., Ciccotti, G., Coker, D. F., Eds.; World Scientific: Singapore, 1998; Chapter 2, pp 25–49.
- (46) Miller, W. H. Classical path approximation for the Boltzmann density matrix. *J. Chem. Phys.* **1971**, 55, 3146–3149.
- (47) Gutzwiller, M. C. In *Chaos in Classical and Quantum Mechanics*; John, F., Kadanoff, L., Marsden, J. E., Sirovich, L., Wiggins, S., Eds.; Interdisciplinary Applied Mathematics; Springer New York: New York, NY, 1990; Vol. 1.
- (48) Landau, L. D.; Lifshitz, E. M. *Mechanics*, 3rd ed.; Course of Theoretical Physics 1; Elsevier, Butterworth-Heinemann: Amsterdam Heidelberg, 2005; pp 2–4.

- (49) Fang, W.; Richardson, J. O.; Chen, J.; Li, X.-Z.; Michaelides, A. Simultaneous deep tunneling and classical hopping for hydrogen diffusion on metals. *Phys. Rev. Lett.* **2017**, *119*, 126001.
- (50) Richardson, J. O. Ring-polymer instanton theory. *Int. Rev. Phys. Chem.* **2018**, *37*, 171–216.